15. N. F. Mott, *Conduction in Non-Crystalline Materials* (Oxford Univ. Press, New York, 1987).
16. A. W. P. Fung, M. S. Dresselhaus, M. Endo, *Phys. Rev. B* **48**, 14953 (1993).
17. D. Belitz and W. Schirmacher, *J. Phys. C* **16**, 913 (1983).
18. M. Kosuka, T. B. Ebbesen, H. Hiura, K. Tanigaki, *Chem. Phys. Lett.* **225**, 161 (1994).

19. We thank P. Stadelmann and B. Senior of the Interdepartmental Electronmicroscopy Center (EPFL) for use of the Philips EM430 microscope and the SEM work, and A. Janossy, L. Zuppiroli, and R. R. Bacsa for stimulating discussions. This work was supported by the Swiss National Fund.

6 December 1994; accepted 21 February 1995

Phonons Localized at Step Edges: A Route to Understanding Forces at Extended Surface Defects

L. Niu, D. J. Gaspar, S. J. Sibener*

Inelastic helium atom scattering has been used to measure the phonons on a stepped metallic crystalline surface, Ni(977). When the scattering plane is oriented parallel to the step edges and perpendicular to the terraces, two branches of step-induced phonons are observed. These branches are identified as transversely polarized, step-localized modes that propagate along the step edge. Analysis reveals significant anisotropy in the force field near the step edge, with all forces near the step edge being substantially smaller than in the bulk. Such measurements provide valuable information on metallic bonding and interface stability near extended surface defects.

The chemical and physical properties of atomic-level surface defects play a crucial role in governing the outcome of many important interfacial processes such as chemical catalysis (*1–4*) and crystal growth (*5–8*). The vibrational characteristics of steps are particularly informative as they provide direct information on the local force field in the vicinity of such defects. These frequencies also provide a stringent test for electronic structure calculations, which seek to quantitatively explain charge redistribution, structural relaxation, and bonding near extended structural defects. Such information will help us to comprehend more fully the role that such defects play in catalysis, corrosion, interface stability, and crystal growth. Moreover, atomic-level steps provide a physical manifestation of a one-dimensional (1D) system that breaks the symmetry of the surrounding 2D environment.

Several recent studies have examined such issues theoretically (*9–14*), but detailed experimental studies of vibrational dynamics on stepped surfaces have been scarce and preliminary in nature (*15–17*). Of particular relevance to this report are the calculations of Berndt *et al.* (*13*), who predicted the existence of two resonant optical branches on stepped surfaces. The few experiments done so far (*15–17*) show modes at or near the surface Brillouin zone (SBZ) center. For example, only one data point could be assigned as a step-localized phonon (at the SBZ center) on Pt(775) (*15*), and only one step-induced phonon branch was observed for Al(221) (*17*). One would ideally like a much more global determination of the vibrational frequencies of step-localized phonons in order to assess fully the bonding interactions along such extended surface defects.

In this report we discuss our observation of two step-localized transverse surface phonon modes that propagate along steps one atom high on a stepped metallic single crystal, Ni(977). We detected these modes by using energy- and momentum-resolved inelastic neutral He atom scattering. These time-of-flight measurements (which can be viewed as a 2D, surface-sensitive analog to inelastic neutron scattering) were carried out with a high-resolution ultrahigh vacuum scattering instrument (energy resolution, 0.46 meV; angular resolution, 0.36°; chopper-to-crystal distance, 55.1 cm; and crystal-to-ionizer distance, 101.5 cm) (Fig. 1A). A more complete description of the instrument can be found elsewhere (*18*). This technique is particularly well suited for this study as the low-energy He atoms do not penetrate into the bulk; that is, they offer superb discrimination between surface and subsurface phenomena. Moreover, He scattering is more sensitive to steps than electron scattering (*19*).

The best way to prepare a high density of (nearly) identical steps is to intentionally cut a crystal surface a few degrees off from a low-Miller-index plane along a specific azimuthal direction. Such vicinal surfaces contain periodically spaced steps of known density and orientation. The Ni(977) surface used in this study, cut at an angle of 7.02° from the (111) surface plane toward the (2$\bar{1}\bar{1}$) direction, consists of eight-atom-wide (111) terraces that are separated by one-atom-high steps of (100) orientation {in microfacet notation (*20*) Ni[8(111)×(100)]}. The crystal orientation used in these experiments was verified to be within 0.5° of the ideal (977) direction with Laue x-ray backreflection. We prepared the crystal by repeated cycles of ion sputtering while cycling the crystal temperature between 400 and 1100 K, followed by annealing at 1100 K. We checked surface cleanliness by Auger spectroscopy, with the largest contaminant, sulfur, being reduced in surface concentration to less than 0.1% coverage. Surface order was confirmed with both low-energy electron and He diffraction. We carefully chose the orientation of the scattering plane, aligned parallel to the steps and perpendicular to the terraces (Fig. 1B), to allow us to spectroscopically resolve the desired step-localized phonon modes.

Step-localized phonons are vibrations that are localized to, and propagate along, the step edges of vicinal surfaces. We can develop an understanding of the polarization characteristics of the normal modes associated with step-localized phonons if we think of a step row of atoms as a 1D lattice with a specific orientation in 3D space, similar to phonons propagating along high symmetry directions in cubic crystals (*21–23*). On the basis of this simple picture, there is a longitudinal mode polarized along the step and two orthogonal transverse modes polarized perpendicular to the step. The transverse polarizations are defined by the symmetry of the stepped surface. One is along the macroscopic surface and perpendicular to the steps (the y direction in Fig. 1B), where there is translational symmetry. The other is the normal to the macroscopic surface (the z direction in Fig. 1B).

In order to successfully detect such step-localized phonons, we have had to delineate the "spectroscopic selection rules" that govern the inelastic scattering dynamics; this task is simplified by a judicious choice of scattering geometry. The scattering plane (denoted by S in Fig. 1B) was chosen parallel to the steps and perpendicular to the terraces. The in-plane scattering of He atoms from terraces was used to precisely orient the crystal. A surface lattice vibration will strongly couple with the He beam if the displacement vector of the vibration has an appreciable projection onto the surface normal. Therefore, He scattering will primarily couple to phonon polarizations that have projections onto the surface normal.

L. Niu, James Franck Institute and the Department of Physics, University of Chicago, 5640 South Ellis Avenue, Chicago, IL 60637, USA.
D. J. Gaspar and S. J. Sibener, James Franck Institute and the Department of Chemistry, University of Chicago, 5640 South Ellis Avenue, Chicago, IL 60637, USA.
*To whom correspondence should be addressed.

How do we spectroscopically resolve the two step-localized transverse modes in an inelastic He atom scattering measurement? To realize this selective detection, we intentionally scatter using either in-phase (Bragg) or out-of-phase (anti-Bragg) diffraction conditions. The in-phase condition, which corresponds to constructive interference between the atom beams specularly scattered ($\theta_i = \theta_f$) from adjacent terraces, satisfies

$$k_i h(\cos\theta_i + \cos\theta_f) = 2k_i h \cos\theta_i = 2n\pi \quad (1)$$

where n is an integer, k_i is the magnitude of the incident momentum, h is the step height in the direction of the terrace normal [2.032 Å for Ni(977)] and θ_i (θ_f) is the incident angle (final angle) with respect to the terrace normal. Similarly, the out-of-phase condition, which corresponds to destructive interference between the atom beams specularly scattered from adjacent terraces, satisfies

$$k_i h(\cos\theta_i + \cos\theta_f) = 2k_i h \cos\theta_i = (2n+1)\pi \quad (2)$$

The z-polarized transverse mode is the most sensitive to changing between in-phase and out-of-phase scattering conditions as it is only 7° from the terrace normal. If we use in-phase conditions, inelastic scattering from the z-polarized step phonon mode will be enhanced as a result of constructive interference effects that influence both the elastic and the inelastic cross sections. This interference becomes destructive when out-of-phase conditions are used. This effect is expected to be much less pronounced for the y-polarized transverse mode because of its limited geometric projection along the scattering plane. Thus, the use of in-phase scattering conditions allows us to selectively detect z-polarized step phonon modes whereas the y-polarized phonon mode signal is too weak to detect. Conversely, the use of out-of-phase conditions allows us to nullify the signal arising from the z-polarized phonon mode, leaving us a window in which to observe (and assign) the y-polarized phonon mode, a predominantly shear horizontal mode that can be detected because of the broken mirror reflection symmetry with respect to the scattering plane. The surface Rayleigh mode would be expected to be

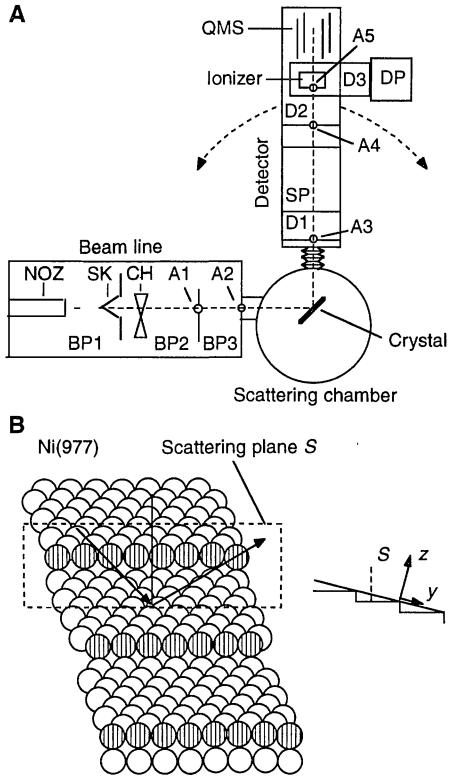

Fig. 1. (**A**) Schematic view of the He scattering apparatus. Conceptually, it consists of three parts: beam line, scattering chamber, and differentially pumped quadrupole-based detector, which rotates about the scattering center. NOZ, nozzle; SK, skimmer; CH, chopper; A, aperture; BP, beam pumping stage; D, detector pumping stage ; SP, spacer; DP, diffusion pump; and QMS, quadrupole mass spectrometer. (**B**) Illustration of the Ni(977) surface including designation of the scattering plane S.

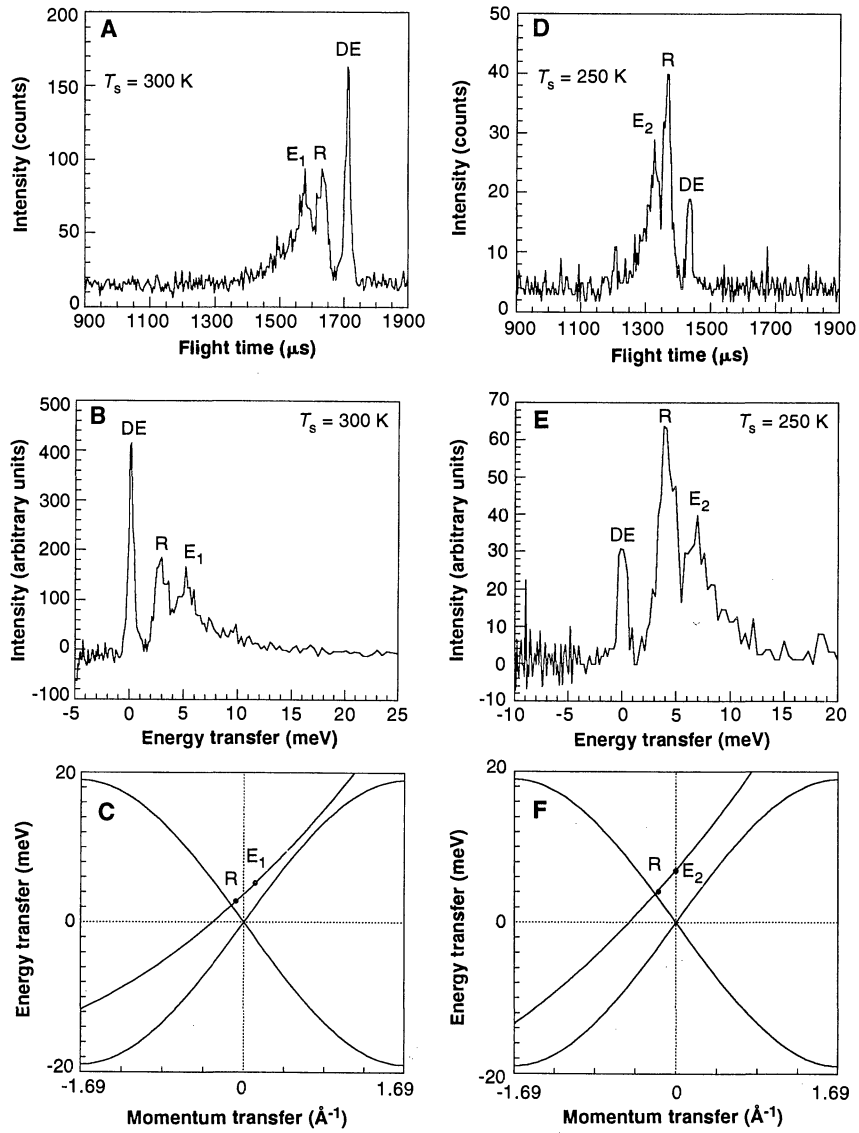

Fig. 2. Time-of-flight spectra that demonstrate the presence of two step-edge phonon modes (E_1 and E_2) observed with the scattering plane oriented along the step direction and perpendicular to the terraces. (**A** to **C**) Plots for in-phase scattering conditions, where (A) is a typical time-of-flight spectrum, (B) shows the data converted to an energy transfer representation, and (C) shows the energy-momentum transfer values associated with E_1 and the Rayleigh wave R along with the associated scan curve (*24*) for the specific experimental conditions (E_i = 17.9 meV, θ_i = 37.4°, and θ_f = 33.4°). DE is the diffuse elastic peak. (**D** to **F**) Corresponding plots under out-of-phase scattering conditions (E_i = 24.4 meV, θ_i = 37.4°, and θ_f = 32.4°), which reveal the location of the other edge-related mode, E_2. Also plotted in (C) and (F) is a sine function representation of the surface Rayleigh mode for Ni(111), scaled using the maximum energy at the $\bar{K}$ point in the SBZ (19.0 meV) measured with inelastic electron scattering (*25*).

visible under both conditions as a result of the large number of terrace atoms. The experimental results presented below confirm the validity of this scattering methodology for selectively studying the dynamical properties of steps.

The primary data in these experiments consist of angle-resolved time-of-flight spectra, which, upon transformation, can be presented in the more informative format of momentum-resolved energy transfer spectra (where positive energy transfer corresponds to phonon annihilation events). Figure 2 shows two examples that confirm the ability of in-phase (Fig. 2, A to C, k_i = 5.84 Å^{-1}) and out-of-phase (Fig. 2, D to F, k_i = 6.81 Å^{-1}) scattering to discriminate between step-induced modes of differing polarization, whereas both kinematic conditions are sensitive to scattering from the Rayleigh wave. The figure progression for in-phase (out-of-phase) scattering, Fig. 2, A to C (Fig. 2, D to F), follows the analysis of momentum- and energy-resolved scattering for a particular Rayleigh wave excitation, R, an "edge mode" phonon, E_1 (E_2), and residual diffuse elastic scattering, DE, a commonly seen incoherent feature in energy-resolved atom scattering.

The phonon excitations shown as points in Fig. 2, C and F, fall on the appropriate scan curves (*24*), which delineate the energy-momentum acceptance conditions of the detector for given kinematic conditions; this leads to unambiguous assignment of the inelastic excitations in a plot of energy versus momentum transfer for Ni(977). Examination of these plots reveals that one inelastic feature in each panel arises from the Rayleigh mode, which propagates along the Ni(111) terraces (*25*); the other excitations, E_1 and E_2, are unique to the stepped surface. These illustrative in-phase and out-of-phase examples were chosen to emphasize that E_1 and E_2 have finite energy at zero momentum, thereby precluding their attribution to the acoustic Rayleigh wave.

In order to definitively assign the nature of the two edge modes, E_1 and E_2, we now plot the full dispersion curves that encompass all of the data we have collected in Fig. 3A; Fig. 3B shows these data in a "folded zone" representation. Note that E_1 and E_2 do not belong to the same phonon dispersion branch; that is, two modes not present on the smooth (111) surface have appeared: E_1 is observed under in-phase conditions and can therefore be assigned as the z-polarized branch, whereas the observation of E_2 under out-of-phase conditions leads to its assignment as the y-polarized step-edge phonon mode. The longitudinal mode of the step is not resolved, perhaps because of its near degeneracy with the surface Rayleigh mode.

Two methods have been used to confirm the step edge nature of these two vibrational modes. The first method is based on the fact that, at slightly elevated temperatures, oxygen preferentially adsorbs at the step edge of Ni(977) in the form of atomic oxygen. This is known from other work in our group dealing with adsorbate-driven step doubling. We have seen that the doubling rate saturates at an O_2 exposure comparable to the double step density, which strongly indicates that oxygen moves to the step edges upon dissociative adsorption (*26*). Because the O atoms preferentially adsorb at the step edges, it is reasonable to expect that such adsorption should preferentially modify the character of step edge–related vibrational modes as compared to the effect on the terrace-related Rayleigh wave. The data shown in Fig. 4, A and B, taken under in-phase conditions,

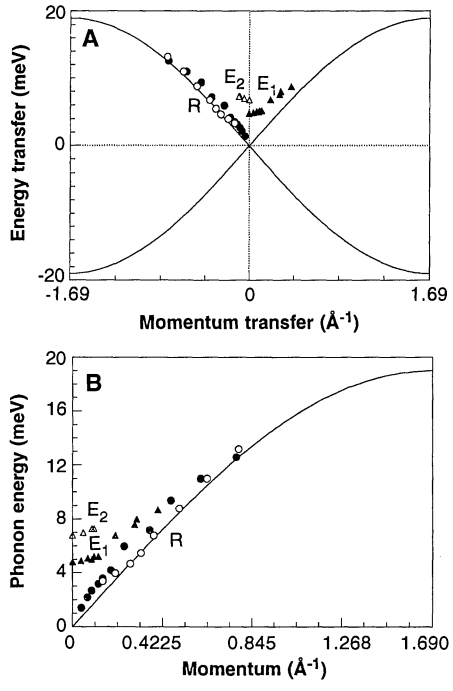

Fig. 3. (**A**) Phonon dispersion data for Ni(977) along the step direction that shows the presence of two step edge–related phonon modes. The solid lines are the Rayleigh mode along the $\bar{\Gamma}\bar{K}$ direction of Ni(111) (see the legend to Fig. 2 for details). Filled symbols represent data taken under in-phase conditions, and open symbols represent data taken under out-of-phase conditions. The circles are due to the Rayleigh mode, and the triangles are the two step edge modes. (**B**) Folded phonon dispersion plot demonstrating the behavior of the two transversely polarized edge modes.

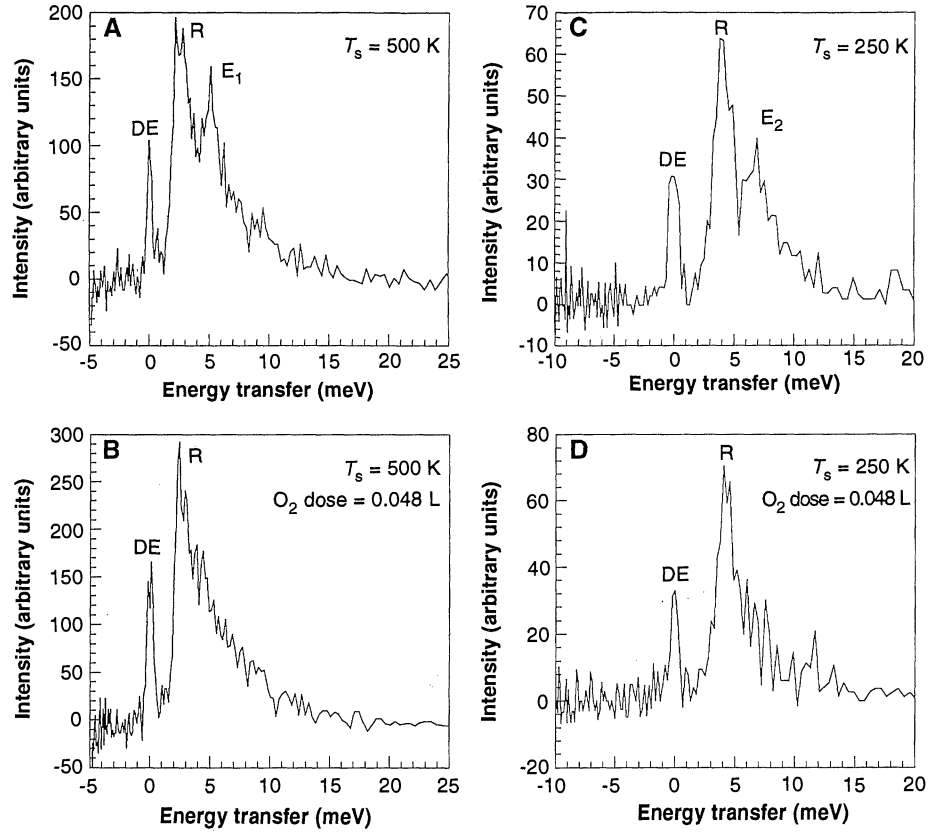

Fig. 4. Adsorbate effects on the two step-induced modes. (**A** and **B**) In-phase scattering data for the clean and O_2-dosed surface. These data demonstrate that small amounts of adsorbed O effectively quench the step edge–localized phonon mode E_1. (**C** and **D**) Out-of-phase scattering data for the clean and O_2-dosed surface. These data demonstrate that small amounts of adsorbed O effectively quench the step edge–localized phonon mode E_2. The data shown in (C) and (D) were taken at 250 K [E_2 disappears at elevated temperatures (see text)]. We first dosed the sample used in (D) with O_2 at a crystal temperature of 500 K before collecting time-of-flight data at 250 K. Scattering conditions were the same as described in Fig. 2.

show spectra that are modified in just the expected manner: We find that an O_2 exposure of 0.048 Langmuir (L) (1 L = 10^{-6} torr·s) quenches the E_1 mode completely while the surface Rayleigh mode persists. Similar results are presented in Fig. 4, C and D, for out-of-phase scattering: An O_2 exposure of 0.048 L quenches the E_2 mode completely while leaving the Rayleigh mode largely unaffected. These observations confirm our assignment of E_1 and E_2 as step edge–induced phonon modes.

The unusually strong temperature sensitivity of the two spectroscopic branches adds further compelling evidence that they are step-edge–induced phonon modes. Our He diffraction measurements of the step structure (*27*) are sensitive to two types of roughening: kink formation in the step row and disordering of the rows neighboring the steps. It has been observed that there is a characteristic onset temperature of ~300 K for kink formation in the row of step atoms and a characteristic onset temperature of 550 K for the disordering of neighboring rows (*27*). Figure 5 shows spectra measured at different crystal temperatures for both in-phase (Fig. 5A) and out-of-phase (Fig. 5B) conditions. We find that E_1 persists until the crystal temperature exceeds 550 K with in-phase conditions. This suggests that the E_1 mode is localized to both the step row and its nearest neighbor rows, so it is not quenched until both are disordered. For out-of-phase conditions, E_2 disappears when the crystal temperature is 300 K or higher, implying that E_2 is more localized at the step row, so that the roughening of the step row (that is, the large-scale formation of kinks) alone quenches the E_2 mode. The surface Rayleigh mode persists above 550 K; it is unaffected by the roughening at the step edges. These temperature dependencies also support our contention that E_1 and E_2 are characterized as step edge–induced modes, although E_2 is more localized than E_1.

To our knowledge, there is no numerical computation available for the dynamics of the Ni(977) surface with which we can directly compare our experimental results. Nevertheless, we find that a simple analytical model, that of a 1D lattice confined in a 2D anisotropic harmonic potential well (*28*), does allow us to estimate the local force field in the vicinity of the steps. At the SBZ center, where $k = 0$, the two new modes correspond to standing wave oscillations governed by the local effective potentials at the step, similar to simple harmonic oscillators with different forces along the y and z directions. Fitting our data to this model yields a force constant for the z direction of $c_z = 5.2$ N/m, and correspondingly, $c_y = 10.4$ N/m along the y direction. (These force constants come from our simple 1D model and will undoubtedly differ somewhat from those extracted from more accurate 3D lattice dynamics or molecular dynamics calculations when they become available; nevertheless, the physical insights provided by the simple model will remain valid.)

Remarkably, the force constant in the y direction is twice that in the z direction, possibly due in part to the difference in the number of the nearest neighbors along these two coordinates. Both values are considerably smaller than the bulk single-force constant of Ni, 37.9 N/m (*29*). This result suggests that the effective forces on the step atoms in the direction perpendicular to steps are greatly softened compared to those of the bulk or the low-Miller-index surfaces of Ni (*29–31*), which have been shown to differ from simple bulk behavior. These findings suggest that substantial electronic charge redistribution occurs at the step edge (*32*), a conclusion that will help to refine our understanding of interface stability, crystal growth, and, at the most fundamental level, charge redistribution in the vicinity of extended structural imperfections on solid surfaces. Ab initio calculations on Ni(977) are needed if we are to understand more fully the origin of these observations.

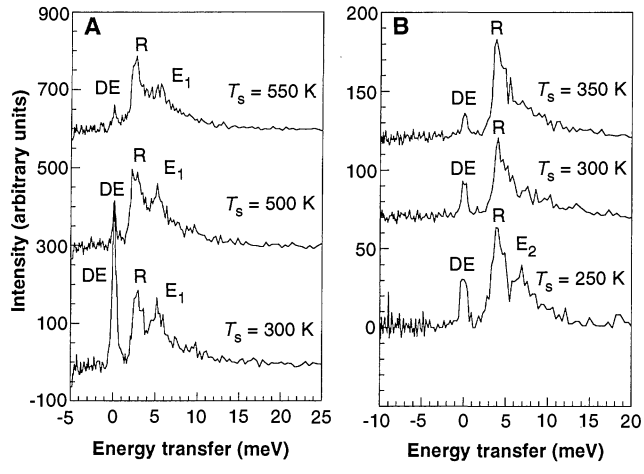

Fig. 5. Temperature sensitivity of the two induced modes. (**A**) In-phase scattering data showing that E_1 persists up to 500 K but becomes attenuated above 550 K. (**B**) Out-of-phase scattering data demonstrating that E_2, which is quite visible at 250 K, essentially vanishes by 300 K. Scattering conditions are the same as those described in Fig. 2.

REFERENCES AND NOTES

1. G. A. Somorjai and D. W. Blakely, *Nature* **258**, 580 (1975).
2. G. A. Somorjai, in *Advances in Catalysis*, D. D. Eley, H. Pines, P. B. Weisz, Eds. (Academic Press, New York, 1977), pp. 2–66.
3. S. S. Fu and G. A. Somorjai, *Surf. Sci.* **262**, 68 (1992).
4. G. A. Somorjai, *ibid.* **299-300**, 849 (1994).
5. O. L. Alerhand *et al.*, *Phys. Rev. Lett.* **64**, 2406 (1990).
6. J. J. de Miguel, C. E. Aumann, R. Kariotis, M. G. Lagally, *ibid.* **67**, 2830 (1991).
7. C. E. Aumann, J. J. de Miguel, R. Kariotis, M. G. Lagally, *Surf. Sci.* **275**, 1 (1992).
8. M. B. Webb, F. K. Men, B. S. Swartzentruber, R. Kariotis, M. G. Lagally, in *Kinetics of Ordering and Growth at Surfaces*, M. G. Lagally, Ed. (Plenum, New York, 1990), pp. 113–124.
9. J. E. Black and P. Bopp, *Surf. Sci.* **140**, 275 (1984).
10. P. Knipp, *Phys. Rev. B* **40**, 7993 (1989).
11. ———, *ibid.* **43**, 6908 (1991).
12. J. E. Black and A. Lock, *Surf. Sci.* **250**, 279 (1991).
13. R. Berndt, A. Lock, C. Woll, *ibid.* **276**, 213 (1992).
14. D. D. Koleske and S. J. Sibener, *J. Electron Spectrosc. Relat. Phenom.* **54-55**, 363 (1990); D. D. Koleske, thesis, University of Chicago (1992).
15. H. Ibach and D. Bruchmann, *Phys. Rev. Lett.* **41**, 958 (1978).
16. M. Wuttig *et al.*, *Surf. Sci.* **193**, 180 (1988).
17. A. Lock, J. P. Toennies, G. Witte, *J. Electron Spectrosc. Relat. Phenom.* **54-55**, 309 (1990).
18. B. Gans, P. A. Knipp, D. D. Koleske, S. J. Sibener, *Surf. Sci.* **264**, 81 (1992). Additional details can be found in the following dissertations: Y. W. Yang, (1988), B. Gans (1990), and S. F. King (1993), all at the University of Chicago. See also Koleske [in (*14*)].
19. A. Lock, B. J. Hinch, J. P. Toennies, in *Kinetics of Ordering and Growth at Surfaces*, M. G. Lagally, Ed. (Plenum, New York, 1990), p. 77.
20. M. A. Van Hove and G. A. Somorjai, *Surf. Sci.* **92**, 489 (1980).
21. A. J. E. Foreman and W. M. Lomer, *Proc. Phys. Soc. London, Sect. B* **70**, 1143 (1957).
22. J. A. Stroscio, M. Persson, C. E. Bartosch, W. Ho, *Phys. Rev. B* **33**, 2879 (1986).
23. M. Persson, J. A. Stroscio, W. Ho, *Phys. Scr.* **36**, 548 (1987).
24. Scan curves are the contours of the conservation of energy and conservation of momentum for specific scattering parameters:

$$\Delta E(\mathbf{Q}) = \frac{\hbar^2}{2m}\left[\left(\frac{k_i \sin\theta_i + \Delta K}{\sin\theta_f}\right)^2 - \mathbf{k}_i^2\right]$$

where $k_i = |\mathbf{k}_i|$ and $\Delta K = \pm|\mathbf{G} + \mathbf{Q}|$ [$\mathbf{G}$ is the surface reciprocal lattice vector, $\mathbf{Q}$ is the momentum transfer to the He atom, m is the mass of the He atom, and $\Delta E(\mathbf{Q})$ is the energy transfer].
25. Unpublished high-resolution electron energy loss spectroscopy results from S.J.S.'s research group; data taken by M. J. Stirniman and W. Li.
26. L. Niu, D. D. Koleske, D. J. Gaspar, S. F. King, S. J. Sibener, in preparation.
27. L. Niu, D. J. Gaspar, S. J. Sibener, in preparation.
28. L. Niu, D. D. Koleske, D. J. Gaspar, S. J. Sibener, *J. Chem. Phys.*, in press.
29. S. Lehwald, F. Wolf, H. Ibach, B. M. Hall, D. L. Mills, *Surf. Sci.* **192**, 131 (1987).
30. S. Lehwald, J. M. Szeftel, H. Ibach, T. S. Rahman, D. L. Mills, *Phys. Rev. Lett.* **50**, 518 (1983).
31. W. Menezes, P. Knipp, G. Tisdale, S. J. Sibener, *Phy. Rev. B* **41**, 5648 (1990).
32. J. S. Nelson and P. J. Feibelman, *Phys. Rev. Lett.* **68**, 2188 (1992).

33. We thank K. Gibson, J. Colonell, and D. Koleske for many helpful discussions. This work was supported by the Air Force Office of Scientific Research and, in part, by the Materials Research Science and Engineering Center Program of the National Science Foundation under award DMR-9400379.

24 October 1994; accepted 24 February 1995